Longitudinal characterization of mGluR5 using ^{11}C-ABP688 PET imaging in the Q175 mouse model of Huntington's disease

Journal of Nuclear Medicine, published on May 24, 2018 as doi:10.2967/jnumed.118.210658

Longitudinal characterization of mGluR5 using ^{11}C-ABP688 PET imaging in the Q175 mouse model of Huntington's disease

Daniele Bertoglio[1§], Lauren Kosten[1§], Jeroen Verhaeghe[1], David Thomae[1,2], Leonie wyffels[1,2], Sigrid Stroobants[1,2], John Wityak[3], Celia Dominguez[3], Ladislav Mrzljak[3], Steven Staelens[1]

[1]Molecular Imaging Center Antwerp (MICA), University of Antwerp, Wilrijk, Belgium
[2]Department of Nuclear Medicine, Antwerp University Hospital, Edegem, Belgium
[3]CHDI Foundation, Princeton, NJ, United States of America
[§]These authors contributed equally to this work.

Corresponding author:

Prof. Steven Staelens
Molecular Imaging Center Antwerp (MICA), Faculty of Medicine and Health Sciences,
University of Antwerp, Universiteitsplein 1, Wilrijk, Belgium
Tel. +32 03265 2820
Email: steven.staelens@uantwerpen.be

First author:

Daniele Bertoglio, PhD Student
Molecular Imaging Center Antwerp (MICA), Faculty of Medicine and Health Sciences,
University of Antwerp, Universiteitsplein 1, Wilrijk, Belgium
Tel. +32 03265 2816
Email: daniele.bertoglio@uantwerpen.be

Financial disclosure

This work was funded by CHDI Foundation, Inc., a non-profit biomedical research organization exclusively dedicated to developing therapeutics that will substantially improve the lives of HD-affected individuals.

Word count: 4964 words

Running title: ^{11}C-ABP688 PET imaging in HD

Keywords: PET; mGluR5; ^{11}C-ABP688; Huntington's disease; Q175

ABSTRACT

The metabotropic glutamate receptor type 5 (mGluR5) represents a potential therapeutic target for the treatment of Huntington's disease (HD). Using ^{11}C-ABP688, a non-competitive and highly selective antagonist for mGluR5, we aimed to longitudinally characterize *in vivo* changes of mGluR5 by means of PET imaging in the Q175 mouse model of HD. **Methods:** ^{11}C-ABP688 PET imaging, followed by an X-ray computed tomography (CT) scan, was performed in heterozygous Q175 mice (n = 18) and wild-type (WT) littermates (n = 18) at three different time points (namely 6, 9, and 13 months of age). ^{11}C-ABP688 binding potential (BP_{ND}) was calculated for each time point in striatum and cortex using the cerebellum as reference region. In addition, voxel-based statistical parametric mapping (SPM) analysis was performed on BP_{ND} images. *Post-mortem* validation of mGluR5 levels and neuronal density was performed at 6 months of age. **Results:** ^{11}C-ABP688 BP_{ND} of heterozygous Q175 animals was significantly reduced at all time points in the striatum (6 months: -13.1%, $p < 0.001$, 9 months: -13.5%, $p < 0.001$, and 13 months: -14.2%, $p < 0.001$) and in the cortex (6 months: -9.8%, $p < 0.01$, 9 months: -10.2%, $p < 0.01$, and 13 months: -10.6%, $p < 0.01$) when compared to WT littermates. Longitudinal changes of ^{11}C-ABP688 BP_{ND} were also found in heterozygous mice showing a reduction at 13 months compared to 6 months (-10.4%, $p < 0.05$). SPM analysis confirmed reduced BP_{ND} in heterozygous compared to WT as well as the time-related decline of ^{11}C-ABP688 binding in the striatum of heterozygous Q175 mice. *Post-mortem* analysis confirmed mGluR5 decrease in both striatum (-36.6%; $p < 0.01$) and cortex (-16.6%; $p < 0.05$) of heterozygous Q175 mice, while no difference in neuronal density was

found. **Conclusion:** *In vivo* imaging of mGluR5 using ^{11}C-ABP688 PET/CT revealed a marked reduction of ligand binding in the striatum and cortex of heterozygous mice compared to WT animals as well as a temporal decline in heterozygous Q175 mice. This study suggests ^{11}C-ABP688 PET imaging as potential biomarker to monitor the disease progression and therapeutic strategies in HD.

INTRODUCTION

Huntington's disease (HD) is an autosomal dominant neurodegenerative disorder characterized by progressive decline in motor function and cognition, and development of psychiatric symptoms (*1*). The disease is caused by an expanded CAG repeat in exon 1 of the gene encoding the protein huntingtin (*2*). Patients with HD exhibit as main neuropathological feature a progressive neuronal cell loss in the caudate-putamen (striatum in rodents) and neocortical regions of the brain (*3*).

Striatal neurons receive input from different areas of the basal ganglia as well as glutamatergic inputs from thalamus and cortex (*4*). Thus, glutamate is postulated to play an important role in the pathogenesis of HD (*5,6*). Stimulation of metabotropic glutamate receptor 5 (mGluR5) results in the formation of inositol 1,4,5-triphosphate (IP_3) and release of intracellular Ca^{2+} (*6,7*). Mutated huntingtin (mHTT) enhances this cell signalling pathway, resulting in toxic levels of intracellular Ca^{2+} and intensified activation of protein kinase C (*7,8*). However, mGluR5 positive modulation can induce activation of neuroprotective cell signalling pathways and promote neuronal survival by activating protein kinase B without inducing Ca^{2+} release (*6,9*). Accordingly, preclinical studies reported that targeting mGluR5 with positive allosteric modulators (PAMs) has a positive effect on memory and cognitive function (*10*) as well as on rescuing pharmacologically-induced memory impairments (*11*). Altogether, these findings suggest a pivotal role of mGluR5 in HD and the potential as therapeutic target to treat HD.

Although several radiotracers have been developed to investigate *in vivo* changes of mGluR5 levels by means of positron emission tomography (PET) imaging (*12*), to date

no *in vivo* studies characterizing mGluR5 levels have been conducted in animal models of HD. PET imaging of mGluR5 provides non-invasive quantitative measure of the receptor expression and can be employed as an effective tool to assess specificity of mGluR5 drugs as well as to evaluate their efficacy longitudinally. Among the mGluR5 PET radiotracers available, ^{11}C-ABP688 (3-(6-methyl-pyridin-2-ylethynyl)-cyclohex-2-enone-O-^{11}C-methyl-oxime) is a potent radiotracer for mGluR5 thanks to its non-competitive, allosteric, high-affinity and highly selective properties (*13*).

In this study, we investigated the PET radiotracer ^{11}C-ABP688 to longitudinally characterize mGluR5 levels during disease progression at 6, 9 and 13 months of age in the recently reported knock-in Q175 animal model for HD (*14,15*). In addition, we quantified mGluR5 and neuronal density at 6 months of age by means of immunohistochemistry in a satellite cohort of animals. The Q175 mouse model of HD displays motor, cognitive, molecular and electrophysiological abnormalities, including *in vivo* temporal decrease in different striatal markers such as dopamine receptors D_1 and $D_{2/3}$, similar to patients with HD (*14-17*).

MATERIAL AND METHODS

Animals

Heterozygous six months old male Q175 knock-in mice (n = 23) and age-matched Q175 wild-type littermates (WT, n = 23) were obtained from Jackson Laboratories (Bar Harbour, Maine, USA). The animals were single-housed in individually ventilated cages under a 12 h light/dark cycle in a temperature- and humidity-controlled environment with

food and water *ad libitum*. All experiments were approved by the Animal Ethics Review Board of University of Antwerp, Belgium (ECD 2014-92). More information regarding the animals is provided in the supplemental materials (available at http://jnm.snmjournals.org).

Tracer Radiosynthesis

^{11}C-ABP688 was prepared using an automated synthesis module (Carbosynthon I, Comecer, The Netherlands). Synthesis of ^{11}C-ABP688 was accomplished by reacting of 0.5 mg desmethyl-ABP688 (E/Z) with [^{11}C]$CH_3SO_3CF_3$ in 400 µl of acetone in presence of 10 µl of NaOH, followed by purification and filtration as previously described (*13*). Average radiochemical purity was 98.40 ± 0.99%, and the specific activity was 75.80 ± 20.41 GBq/µmol.

^{11}C-ABP688 Dynamic MicroPET Scan

MicroPET/Computed tomography (CT) imaging was performed on two Siemens Inveon PET-CT scanners (Siemens Preclinical Solution, USA) at 6, 9, and 13 months of age. The animals were anaesthetized using isoflurane (Forene, Belgium) in medical oxygen (induction 5%, maintenance 1.5%). Animals were catheterized in the tail vein for intravenous (i.v.) bolus injection of the tracer and positioned onto the scanner. Respiration and heart rate of the animal were constantly monitored using a Monitoring Acquisition Module (Minerve, France) during the entire scanning period. Body

temperature of the animals was maintained at 37 ± 1°C using a feedback-controlled warm air flow (Minerve, France).

At the onset of the 60 min dynamic microPET scan, mice were injected with a bolus of ^{11}C-ABP688 over a 12 second interval (1 ml/min) using an automated pump (Pump 11 Elite, Harvard Apparatus, USA). Tracer activity was injected keeping the cold dose within tracer conditions (<1.50 µg/kg). PET data were acquired in list mode. Following the microPET scan, a 10 min 80 kV/500 µA CT scan was performed for attenuation and scatter correction. During the progression of the disease, average body weight was significantly reduced in heterozygous Q175 mice at 9 (-10.0%; $p < 0.001$) and 13 (-15.8%; $p < 0.0001$) months of age when compared to WT Q175 mice (Supplemental Table 1). Additional data on the weight of the animals, injected radioactivity levels, injected mass, and number of animals for each time point can be found in supplemental table 1.

Image Processing And Analysis

Acquired PET images were histogrammed and reconstructed into 33 frames of increasing duration (12x10 s, 3x20 s, 3x30 s, 3x60 s, 3x150 s and 9x300 s). Iterative PET image reconstruction of the images was performed using 4 iterations and 16 subsets of the 2-dimensional ordered-subset expectation maximization (2D-OSEM) algorithm (*18*) following Fourier rebinning. Normalization, dead time, CT-based attenuation and single-scatter simulation scatter corrections were applied. PET image frames were reconstructed on a 128 x 128 x 159 grid with 0.776 x 0.776 x 0.796 mm^3. Images are

represented as averages over the group (heterozygous and WT) in in selected coronal/sagittal/transversal slices mouse brain view.

PET images were processed and analysed using PMOD 3.6 software (Pmod Technologies, Zurich, Switzerland) for any regional and voxel-based analysis. A ^{11}C-ABP688 PET template based on data of WT animals was used for quantification as we have previously shown the ^{11}C-ABP688 PET template results in reproducible and reliable quantification in mice (in-house data). Using the predefined volume-of-interest (VOI) template, time activity curves (TACs) of different regions (striatum, cortex and cerebellum) were extracted from the image. Following kinetic modelling, the non-displaceable binding potential BP_{ND} for these regions was calculated using the simplified reference tissue model (SRTM) (*19*) with the cerebellum as reference tissue as we have previously validated in mice (in-house data). PET images were smoothed using an isotropic Gaussian filter (FWHM = 0.5 mm) and a voxel-based analysis with Statistical Parametric Mapping (SPM) was performed using SPM12 (Wellcome Department of Imaging Neuroscience, London, UK). For SPM analysis, data obtained from heterozygous and WT Q175 mice without missing observations were compared (WT vs heterozygous). Statistical T-maps were calculated for a peak voxel threshold of $p = 0.05$ (uncorrected) and cluster threshold of 100 voxels (0.8 mm^3). Only significant clusters with $p < 0.05$ were considered and reported.

Immunohistochemistry

mGluR5 immunohistochemistry was performed to confirm *in vivo* changes in mGluR5 levels, while neuronal nuclei (NeuN) immunostaining was aimed at quantifying neuronal density as previously reported (*20*). A detailed description of the methodology is provided in the supplemental materials.

Statistical Analysis

Normal distribution of data was assessed using the Shapiro-Wilk test to confirm normality. Longitudinal analysis was performed with a linear-mixed model, which did not require exclusion of animals if a measurement was missing as this method takes into account missing observations. Detailed description of the linear mixed model is provided in the supplemental materials.

Since sample size was too low to estimate normality, Mann-Whitney U test was used to investigate differences between genotypes in the immunohistochemistry analysis. Normality test and *post-mortem* analyses were performed with GraphPad Prism (v 6.0) statistical software, while linear mixed model analysis was performed in JMP Pro 13 (SAS). The data are represented as mean ± standard deviation (SD). All tests were two-tailed, except for SPM analysis (one-tailed), and significance was set at $p < 0.05$.

RESULTS

Small Animal ^{11}C-ABP688 PET Imaging

Average microPET images of ^{11}C-ABP688 BP_{ND} for heterozygous and WT mice at each time point are displayed in Fig. 1. At 6 months of age, the ^{11}C-ABP688 BP_{ND} was

significantly reduced in heterozygous animals compared to WT littermates in striatum (WT = 1.22 ± 0.10, heterozygous = 1.06 ± 0.15; -13.1 ± 2.3%, $p < 0.001$) as well as in cortex (WT = 0.80 ± 0.08 and heterozygous = 0.72 ± 0.09; -9.8 ± 2.1%, $p < 0.01$) (Fig. 2). Consistently, at 9 months of age, ^{11}C-ABP688 BP_{ND} values were significantly lower in heterozygous mice compared to WT littermates in both striatum (WT = 1.17 ± 0.13 and heterozygous = 1.01 ± 0.10; -13.5 ± 2.4%, $p < 0.001$) and cortex (WT = 0.77 ± 0.07 and heterozygous = 0.69 ± 0.07; -10.2 ± 2.2%, $p < 0.01$) (Fig. 2). Finally, at 13 months of age, the ^{11}C-ABP688 BP_{ND} decrease in heterozygous mice compared to WT littermates was significant in both striatum (WT = 1.11 ± 0.12 and heterozygous = 0.95 ± 0.13; -14.2 ± 2.5%, $p < 0.001$) and cortex (WT = 0.75 ± 0.08 and heterozygous = 0.66 ± 0.10; -10.6 ± 2.3%, $p < 0.01$) (Fig. 2).

A significant progressive temporal decline of ^{11}C-ABP688 BP_{ND} was found in the striatum of heterozygous animals between 6 and 13 months of age (-10.4% ± 3.2%, $p < 0.05$) (Fig. 2). On the contrary, no significant reduction of ^{11}C-ABP688 BP_{ND} was found in WT littermates between 6 and 13 months of age (-6.1% ± 2.3%, $p > 0.05$).

Voxel-based analysis confirmed the decreased binding in striatum of heterozygous mice compared to WT littermates already at 6 months of age (Fig. 3). In addition, the voxel-based analysis reflected the time-related decline of ^{11}C-ABP688 binding in striatum of heterozygous at 9 and 13 months of age (Fig. 3).

Immunohistochemistry

In agreement with ^{11}C-ABP688 PET imaging, mGluR5 immunoreactivity at 6 months of age was significantly reduced in heterozygous mice when compared to WT littermates in both striatum (WT = 7.75 ± 1.21 x10^8 and heterozygous = 4.91 ± 0.51 x10^8; -36.6%; $p < 0.01$) and cortex (WT = 2.57 ± 0.27 x10^8 and heterozygous = 2.14 ± 0.19 x10^8; -16.6%; $p < 0.05$) (supplemental Fig. 1).

On the contrary, no statistical significant difference in neuronal density was found between WT and heterozygous Q175 mice in both striatum (WT = 91.0 ± 5.6 NeuN counts/µm^2 and heterozygous = 87.1 ± 6.9 NeuN counts/µm^2, -4.2%; $p = 0.42$) and cortex (WT = 108.1 ± 5.3 NeuN counts/µm^2 and heterozygous = 109.4 ± 5.7 NeuN counts/µm^2, +1.2%; $p = 0.42$) (supplemental Fig. 2).

DISCUSSION

The present study aimed at investigating the changes in mGluR5 levels during disease progression in the Q175 mouse model of HD with the PET radioligand ^{11}C-ABP688 as a potential biomarker for disease progression in HD. To the best of our knowledge, this is the first *in vivo* study to image mGluR5 longitudinally in an animal model of HD. Our findings indicated that ^{11}C-ABP688, given its non-competitive, allosteric, high-affinity and highly selective properties, is a promising radiotracer for imaging changes in mGluR5 levels during the progression of HD. In particular, longitudinal PET quantification of ^{11}C-ABP688 revealed a marked reduction of ligand binding in the striatum and cortex of heterozygous mice compared to WT littermates. Consistently, *post-mortem* analysis at 6

months of age resulted in a significant decline in mGluR5 levels in both striatum and cortex of heterozygous Q175 mice. Noteworthy, no significant difference in neuronal density was found, suggesting the decrease in mGluR5 density was not simply related to loss of neurons, but more likely to a downregulation of the receptor availability. Accordingly, *in vitro* ^{11}C-ABP688 and ^{3}H-ABP688 autoradiography in *post-mortem* human brain tissue demonstrated a significant decrease in mGluR5 density in HD patients compared to controls (*21*).

One possible limitation of the current study was the lack of magnetic resonance images (MRI). Although MRI might result critical in the co-registration of certain radiotracers, we previously investigated its benefit for ^{11}C-ABP688 and found a nearly perfect agreement in the quantification based on either MRI or ^{11}C-ABP688 PET template (striatum: $r = 0.989$; $r^2 = 0.978$) (in-house data), thus we excluded MRI in order to reduce as much as possible the number of anaesthesia sessions.

mGluR5 is highly expressed in brain regions affected in HD, including striatum and cortex (*22*) and its expression is altered in knock-in mouse model of HD (*23*) as well as human samples (*21*). In addition, mGluR5 is involved in movement control as mGluR5 knockout mice display enhanced locomotor activity with HD-related pathology (*24*). Notably, mGluR5 can physically interact with WT and mutant HTT and HTT can modulate mGluR1/5 signalling (*25*). Altogether, these findings suggest that mGluR5 represents a potential biomarker and candidate therapeutic target in HD. However, further understanding is necessary to determine whether mGluR5 activation either slows or aggravates the development HD pathology, as mGluR5 signalling may result in either

activation of neuroprotective pathways or neuronal toxicity (*26*). This duality translates in two opposite strategies, both with the potential to treat HD: on one hand, PAMs can ameliorate pathology and phenotype in HD mice (*9,27*) by inducing activation of neuroprotective cell signalling pathways through the activation of protein kinase B; on the other hand, negative allosteric modulators (NAMs) could be an alternative viable strategy for treating HD since mHTT contributes to the enhancement of mGluR5 pathway, resulting in toxic levels of intracellular Ca^{2+} and intensified activation of protein kinase C (*7,8*). Accordingly, mGluR5 knockout reverses neuropathology and improves the motor function of HD mice (*24*) and NAMs attenuate motor coordination decline as well as improve clearance of mHTT aggregates in HD mice, possibly by enhancing the autophagy-mediated scavenger activity (*28,29*).

Even though mGluR5 appears to be markedly involved in the disease progression of HD, to date no studies have been conducted to investigate mGluR5 longitudinal changes in animal models of HD. The striking reduction of mGluR5 levels we demonstrated over time suggests ^{11}C-ABP688 PET imaging as biomarker of disease progression in HD. In addition, it could be used to evaluate the effect of treatments targeting mGluR5 (NAMs or PAMs) in treating HD as well as to evaluate the effect of HTT-lowering therapeutic agents on mGluR5 levels. For instance, treatment with cystamine, inhibitor of transglutaminase, enzyme involved in the formation of mHTT, had proven its efficacy (*30*) therefore ^{11}C-ABP688 PET imaging during therapy could provide insights on the mechanism of mGluR5 in HD.

Nonetheless, mGluR5 PET imaging warrants cautions and needs to be carefully planned to guarantee adequate statistical power. In this study, we found a statistically significant temporal decline of mGluR5 levels in heterozygous Q175 mice in agreement with the progression of the disease. However, the absolute percentage change of mGluR5 levels between heterozygous and WT Q175 in both investigated regions showed only negligible differences between time points (e.g. in striatum = -13.1%, -13.5% and -14.2% at 6, 9, and 13 months, respectively). This might be associated to a relative decline in mGluR5 density with aging, which has been previously reported in rodents (*31-33*). In the present study, only an age-related trend was found in WT mice (e.g. in striatum between 6 and 13 months of age = -6.1% ± 2.3%; $p > 0.05$). Nevertheless, a recent study in humans did not show age-related difference in ^{11}C-ABP688 binding potential (*34*).

However, several studies indicated that mGluR5 availability might differ on daily basis. In particular, Elmenhorst and colleagues reported a circadian variation of mGluR5 availability in the rat brain showing an increase up to 10% during the sleep phase (*35*). Similarly, test-retest studies for ^{11}C-ABP688 PET quantification reported *in vivo* variation of mGluR5 levels in non-human primates (*36*) and in humans (*37,38*), possibly due to changes in endogenous glutamate levels during the day, although this was not found in rats (*39*). A possible explanation could be the use of isoflurane anaesthesia during rodent studies, thus it might be of interest to investigate mGluR5 levels with an awake scan paradigm to further examine ^{11}C-ABP688 translational significance. Nevertheless, ^{11}C-ABP688 test-retest studies performed on different days indicate that this tracer provides reliable outcome measures in rodents (*40*) (in-house data) as well as in humans (*41*).

Furthermore, a previous study reported that mGluR5 levels are altered in humans following sleep deprivation, with a global increase in mGluR5 binding in subjects sleep-deprived when compared to subjects with regular sleep (*42*). A relevant finding since sleep disturbance has been reported as one of the earliest abnormalities in patient with premanifest HD (*43*) and confirmed in animal models of HD (*44,45*). Overall, these variables need to be carefully considered when evaluating ^{11}C-ABP688 as potential biomarker in HD patients in order to avoid possible confounding factors limiting the statistical power of future studies.

^{11}C-ABP688 PET imaging is a promising biomarker to monitor HD disease progression. This is related to the fact that mGluR5 levels change during the disease and these changes are not only related to neuronal loss in the striatum, but also to direct interaction of mHTT with mGluR5 function.

CONCLUSION

This study suggests ^{11}C-ABP688 PET imaging as potential biomarker to monitor the disease progression of HD with prospective application to humans. In addition, disease-related decrease in mGluR5 levels could be helpful either as potential translational biomarker for disease progression studies or as readout to evaluate disease-modifying treatments.

ACKNOWLEDGEMENTS

D. Bertoglio has a PhD fellowship from the Research Foundation Flanders (FWO, 11W2516N/11W2518N). The authors thank Philippe Joye and Caroline Berghmans of the Molecular Imaging Center Antwerp (MICA) for their expertise and valuable technical assistance. This work was supported by CHDI Foundation, Inc., a non-profit biomedical research organization exclusively dedicated to developing therapeutics that will substantially improve the lives of HD-affected individuals.

DISCLOSURE

This work was funded by CHDI Foundation, Inc., a non-profit biomedical research organization exclusively dedicated to developing therapeutics that will substantially improve the lives of HD-affected individuals. No other potential conflict of interest relevant to this article was reported.

SUPPLEMENTAL DATA

Supplementary data to this article can be found online (available at http://jnm.snmjournals.org).

REFERENCES

1. Brandt J, Butters N. The neuropsychology of Huntington's disease. *Trends Neurosci.* 1986:118-120.

2. Group THsDCR. A novel gene containing a trinucleotide repeat that is expanded and unstable on Huntington's disease chromosomes. *Cell.* 1993:971-983.

3. Vonsattel JP, Myers RH, Stevens TJ, Ferrante RJ, Bird ED, Richardson EP, Jr. Neuropathological classification of Huntington's disease. *J Neuropathol Exp Neurol.* 1985;44:559-577.

4. Joel D, Weiner I. The organization of the basal ganglia-thalamocortical circuits: open interconnected rather than closed segregated. *Neuroscience.* 1994;63:363-379.

5. DiFiglia M. Excitotoxic injury of the neostriatum: a model for Huntington's disease. *Trends Neurosci.* 1990;13:286-289.

6. Ribeiro FM, Paquet M, Cregan SP, Ferguson SS. Group I metabotropic glutamate receptor signalling and its implication in neurological disease. *CNS Neurol Disord Drug Targets.* 2010;9:574-595.

7. Tang TS, Slow E, Lupu V, et al. Disturbed Ca2+ signaling and apoptosis of medium spiny neurons in Huntington's disease. *Proc Natl Acad Sci U S A.* 2005;102:2602-2607.

8. Tang TS, Tu H, Chan EY, et al. Huntingtin and huntingtin-associated protein 1 influence neuronal calcium signaling mediated by inositol-(1,4,5) triphosphate receptor type 1. *Neuron.* 2003;39:227-239.

9. Doria JG, Silva FR, de Souza JM, et al. Metabotropic glutamate receptor 5 positive allosteric modulators are neuroprotective in a mouse model of Huntington's disease. *Br J Pharmacol.* 2013;169:909-921.

10. Ayala JE, Chen Y, Banko JL, et al. mGluR5 positive allosteric modulators facilitate both hippocampal LTP and LTD and enhance spatial learning. *Neuropsychopharmacology.* 2009;34:2057-2071.

11. Reichel CM, Schwendt M, McGinty JF, Olive MF, See RE. Loss of object recognition memory produced by extended access to methamphetamine self-administration is reversed by positive allosteric modulation of metabotropic glutamate receptor 5. *Neuropsychopharmacology.* 2011;36:782-792.

12. Pillai RL, Tipre DN. Metabotropic glutamate receptor 5 - a promising target in drug development and neuroimaging. *Eur J Nucl Med Mol Imaging.* 2016;43:1151-1170.

13. Ametamey SM, Kessler LJ, Honer M, et al. Radiosynthesis and preclinical evaluation of 11C-ABP688 as a probe for imaging the metabotropic glutamate receptor subtype 5. *J Nucl Med.* 2006;47:698-705.

14. Heikkinen T, Lehtimaki K, Vartiainen N, et al. Characterization of neurophysiological and behavioral changes, MRI brain volumetry and 1H MRS in zQ175 knock-in mouse model of Huntington's disease. *PLoS One.* 2012;7:e50717.

15. Menalled LB, Kudwa AE, Miller S, et al. Comprehensive behavioral and molecular characterization of a new knock-in mouse model of Huntington's disease: zQ175. *PLoS One.* 2012;7:e49838.

16. Peng Q, Wu B, Jiang M, et al. Characterization of Behavioral, Neuropathological, Brain Metabolic and Key Molecular Changes in zQ175 Knock-In Mouse Model of Huntington's Disease. *PLoS One.* 2016;11:e0148839.

17. Haggkvist J, Toth M, Tari L, et al. Longitudinal microPET imaging of the zQ175 mouse model of Huntington's disease shows in vivo changes of molecular targets in the striatum and the cerebral cortex. *J Nucl Med.* 2016.

18. Hudson HM, Larkin RS. Accelerated image reconstruction using ordered subsets of projection data. *IEEE Trans Med Imaging.* 1994;13:601-609.

19. Lammertsma AA, Hume SP. Simplified reference tissue model for PET receptor studies. *Neuroimage.* 1996;4:153-158.

20. Bertoglio D, Amhaoul H, Van Eetveldt A, et al. Kainic Acid-Induced Post-Status Epilepticus Models of Temporal Lobe Epilepsy with Diverging Seizure Phenotype and Neuropathology. *Front neurol.* 2017;8:1-13.

21. Gulyas B, Sovago J, Gomez-Mancilla B, et al. Decrease of mGluR5 receptor density goes parallel with changes in enkephalin and substance P immunoreactivity in Huntington's disease: a preliminary investigation in the postmortem human brain. *Brain Struct Funct.* 2015;220:3043-3051.

22. Shigemoto R, Nomura S, Ohishi H, Sugihara H, Nakanishi S, Mizuno N. Immunohistochemical localization of a metabotropic glutamate receptor, mGluR5, in the rat brain. *Neurosci Lett.* 1993;163:53-57.

23. Ribeiro FM, Paquet M, Ferreira LT, et al. Metabotropic glutamate receptor-mediated cell signaling pathways are altered in a mouse model of Huntington's disease. *J Neurosci.* 2010;30:316-324.

24. Ribeiro FM, Devries RA, Hamilton A, et al. Metabotropic glutamate receptor 5 knockout promotes motor and biochemical alterations in a mouse model of Huntington's disease. *Hum Mol Genet.* 2014;23:2030-2042.

25. Anborgh PH, Godin C, Pampillo M, et al. Inhibition of metabotropic glutamate receptor signaling by the huntingtin-binding protein optineurin. *J Biol Chem.* 2005;280:34840-34848.

26. Ribeiro FM, Hamilton A, Doria JG, Guimaraes IM, Cregan SP, Ferguson SS. Metabotropic glutamate receptor 5 as a potential therapeutic target in Huntington's disease. *Expert Opin Ther Targets.* 2014;18:1293-1304.

27. Doria JG, de Souza JM, Andrade JN, et al. The mGluR5 positive allosteric modulator, CDPPB, ameliorates pathology and phenotypic signs of a mouse model of Huntington's disease. *Neurobiol Dis.* 2015;73:163-173.

28. Schiefer J, Sprunken A, Puls C, et al. The metabotropic glutamate receptor 5 antagonist MPEP and the mGluR2 agonist LY379268 modify disease progression in a transgenic mouse model of Huntington's disease. *Brain Res.* 2004;1019:246-254.

29. Abd-Elrahman KS, Hamilton A, Hutchinson SR, Liu F, Russell RC, Ferguson SSG. mGluR5 antagonism increases autophagy and prevents disease progression in the zQ175 mouse model of Huntington's disease. *Sci Signal.* 2017;10:1-11.

30. Wang X, Sarkar A, Cicchetti F, et al. Cerebral PET imaging and histological evidence of transglutaminase inhibitor cystamine induced neuroprotection in transgenic R6/2 mouse model of Huntington's disease. *J Neurol Sci.* 2005;231:57-66.

31. Fang XT, Eriksson J, Antoni G, et al. Brain mGluR5 in mice with amyloid beta pathology studied with in vivo [11C]ABP688 PET imaging and ex vivo immunoblotting. *Neuropharmacology.* 2017;113:293-300.

32. Domenici MR, Pintor A, Potenza RL, et al. Metabotropic glutamate receptor 5 (mGluR5)-mediated phosphoinositide hydrolysis and NMDA-potentiating effects are blunted in the striatum of aged rats: a possible additional mechanism in striatal senescence. *Eur J Neurosci.* 2003;17:2047-2055.

33. Canas PM, Duarte JM, Rodrigues RJ, Kofalvi A, Cunha RA. Modification upon aging of the density of presynaptic modulation systems in the hippocampus. *Neurobiol Aging.* 2009;30:1877-1884.

34. DuBois JM, Rousset OG, Rowley J, et al. Characterization of age/sex and the regional distribution of mGluR5 availability in the healthy human brain measured by high-resolution [(11)C]ABP688 PET. *Eur J Nucl Med Mol Imaging.* 2016;43:152-162.

35. Elmenhorst D, Mertens K, Kroll T, et al. Circadian variation of metabotropic glutamate receptor 5 availability in the rat brain. *J Sleep Res.* 2016;25:754-761.

36. Sandiego CM, Nabulsi N, Lin SF, et al. Studies of the metabotropic glutamate receptor 5 radioligand [(1)(1)C]ABP688 with N-acetylcysteine challenge in rhesus monkeys. *Synapse.* 2013;67:489-501.

37. DeLorenzo C, Kumar JS, Mann JJ, Parsey RV. In vivo variation in metabotropic glutamate receptor subtype 5 binding using positron emission tomography and [11C]ABP688. *J Cereb Blood Flow Metab.* 2011;31:2169-2180.

38. DeLorenzo C, Gallezot JD, Gardus J, et al. In vivo variation in same-day estimates of metabotropic glutamate receptor subtype 5 binding using [11C]ABP688 and [18F]FPEB. *J Cereb Blood Flow Metab.* 2016:271678X16673646.

39. Wyckhuys T, Verhaeghe J, Wyffels L, et al. N-acetylcysteine- and MK-801-induced changes in glutamate levels do not affect in vivo binding of metabotropic glutamate 5 receptor radioligand 11C-ABP688 in rat brain. *J Nucl Med.* 2013;54:1954-1961.

40. Elmenhorst D, Aliaga A, Bauer A, Rosa-Neto P. Test-retest stability of cerebral mGluR(5) quantification using [(1)(1)C]ABP688 and positron emission tomography in rats. *Synapse.* 2012;66:552-560.

41. Burger C, Deschwanden A, Ametamey S, et al. Evaluation of a bolus/infusion protocol for 11C-ABP688, a PET tracer for mGluR5. *Nucl Med Biol.* 2010;37:845-851.

42. Hefti K, Holst SC, Sovago J, et al. Increased metabotropic glutamate receptor subtype 5 availability in human brain after one night without sleep. *Biol Psychiatry.* 2013;73:161-168.

43. Lazar AS, Panin F, Goodman AO, et al. Sleep deficits but no metabolic deficits in premanifest Huntington's disease. *Ann Neurol.* 2015;78:630-648.

44. Loh DH, Kudo T, Truong D, Wu Y, Colwell CS. The Q175 mouse model of Huntington's disease shows gene dosage- and age-related decline in circadian rhythms of activity and sleep. *PLoS One.* 2013;8:e69993.

45. Kantor S, Szabo L, Varga J, Cuesta M, Morton AJ. Progressive sleep and electroencephalogram changes in mice carrying the Huntington's disease mutation. *Brain.* 2013;136:2147-2158.

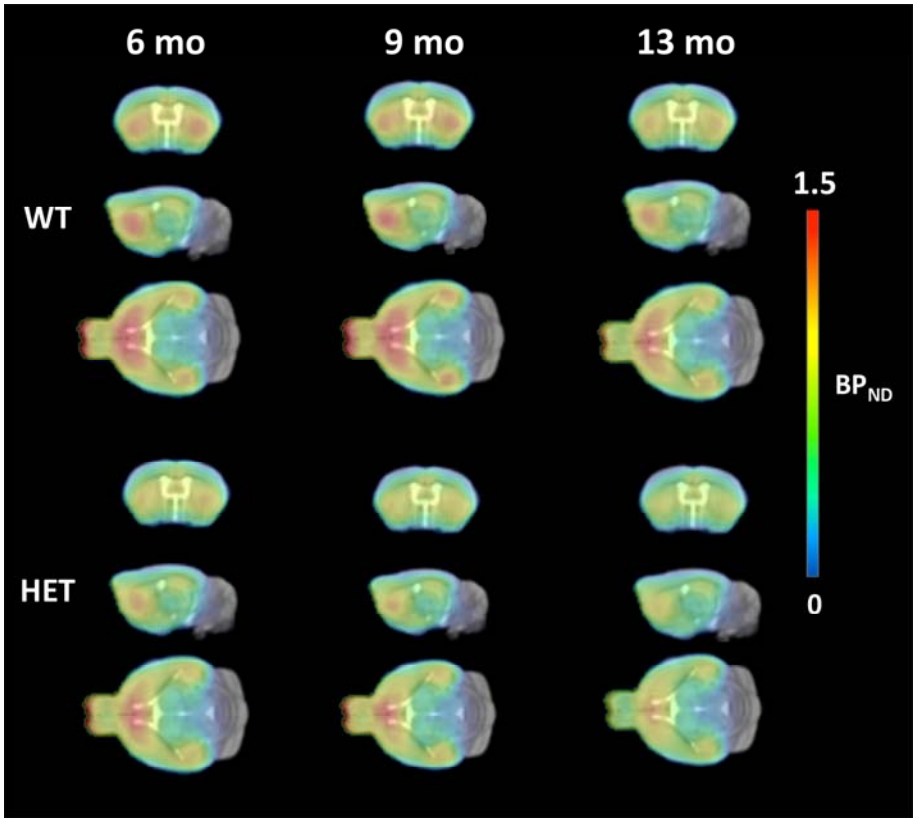

FIGURE 1. Longitudinal imaging of ^{11}C-ABP688 uptake in WT and heterozygous Q175 mice. Average microPET images of ^{11}C-ABP688 BP_{ND} in WT and heterozygous at each time point. microPET images are overlaid onto a MRI mouse brain template for anatomical localization. 6 months (WT, *n* = 15; heterozygous, *n* = 16), 9 months (WT, *n* = 15; heterozygous, *n* = 12), 13 months (WT, *n* = 12; heterozygous, *n* = 15). WT = wild-type, HET = heterozygous, mo = months.

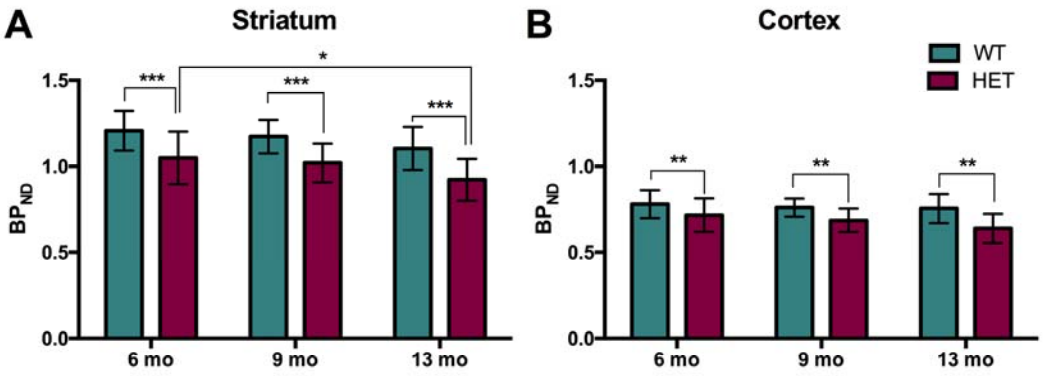

FIGURE 2. Heterozygous Q175 mice demonstrated reduced ^{11}C-ABP688 BP_{ND} values compared to WT in both striatum (**A**) and cortex (**B**) as well as an age-related BP_{ND} decrease in striatum. WT, *n* = 15; heterozygous, *n* = 16. **p* < 0.05, ***p* < 0.01, ****p* < 0.001. WT = wild-type, HET = heterozygous, mo = months.

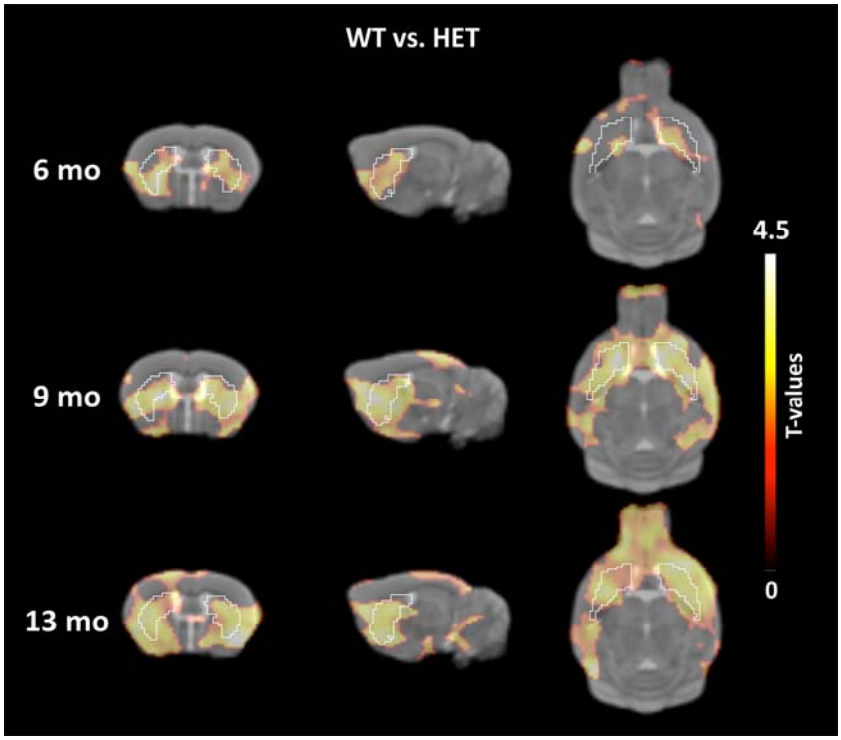

FIGURE 3. SPM results comparing ^{11}C-ABP688 PET signal intensity of heterozygous (*n* = 12) and WT (n = 12) Q175 mice. Statistical map of T-values (threshold $p < 0.05$ (uncorrected) and a cluster threshold of 100 voxels (0.8 mm^3)) overlaid onto a MRI mouse brain template for anatomical localization showing clusters of reduced ^{11}C-ABP688 uptake in heterozygous mice compared to WT animals (WT > heterozygous). WT = wild-type, HET = heterozygous, mo = months.

Longitudinal characterization of mGluR5 using ^{11}C-ABP688 PET imaging in the Q175 mouse model of Huntington's disease

Daniele Bertoglio[1§], Lauren Kosten[1§], Jeroen Verhaeghe[1], David Thomae[1,2], Leonie wyffels[1,2], Sigrid Stroobants[1,2], John Wityak[3], Celia Dominguez[3], Ladislav Mrzljak[3], Steven Staelens[1]

[1]Molecular Imaging Center Antwerp (MICA), University of Antwerp, Wilrijk, Belgium
[2]Department of Nuclear Medicine, Antwerp University Hospital, Edegem, Belgium
[3]CHDI Foundation, Princeton, NJ, United States of America
[§]These authors contributed equally to this work.

SUPPLEMENTAL INFORMATION

MATERIAL AND METHODS

Animals

Heterozygous six months old male Q175 knock-in mice (*n* = 23) containing the human mutant HTT (mHTT) allele with the expanded CAG repeat within the native mouse Huntington gene (*1*) and age-matched Q175 wild-type littermates (WT, *n* = 23) were obtained from Jackson Laboratories (Bar Harbour, Maine, USA). Since homozygousity is rare in patients, HET mice were chosen to better resemble the clinical condition. The recently developed Q175 mouse model was preferred over the well-reported R6/2 HD model given the slower disease progression that more closely mimics HD in humans and provides more opportunities for testing disease-modifying therapies. Eighteen animals per genotype were included in the longitudinal study, while 5 separate mice per genotype were sacrificed at 6 months of age for post-*mortem* quantification of mGluR5 and neuronal density. The animals were single-housed in individually ventilated cages under a 12 h light/dark cycle in a temperature- and humidity-controlled environment with food

and water *ad libitum*. Single-housing was required to avoid the development of dominant-subdominant and aggressive behaviour. The animals were acclimatized to the facility for at least one week before the start of procedures. All experiments were approved by the Animal Ethics Review Board of University of Antwerp, Belgium (ECD 2014-92). All applicable European Committee Guidelines (decree 2010/63/CEE) and the Animal Welfare Act (7 USC 2131) for the care and use of animals were followed.

Immunohistochemistry

Animals were sacrificed by decapitation and brains were quickly removed and fresh-frozen in 2-metylbuthane at -35°C for 2 minutes and further preserved at -20°C until staining. Serial coronal sections (20 µm of thickness) were collected starting at 5.34 mm from bregma (*2*) to cover the striatum, in triplicate on Superfrost Plus slides (Thermo Fischer Scientific, USA), using a cryostat (Leica, Germany).

mGluR5 immunohistochemistry was performed to confirm *in vivo* changes in mGluR5 levels, while neuronal nuclei (NeuN) immunostaining was aimed at quantifying neuronal density as previously reported (*3*).

Slides were fixed in 4% paraformaldehyde for 10 min and, following rinses in PBS (pH 7.4), were immersed in water containing 3% H_2O_2 for 5 min to quench endogenous peroxidases. Then, for mGluR5 IHC, blocking solution containing 10% normal goat serum (NGS) and 0.3% Triton X-100 in PBS was added for 1 h. After 3 washes in PBS, avidin was added to the sections for 15 min, rinsed briefly and subsequently blocked with biotin for 15 min, followed by incubation with polyclonal mGluR5 primary antibody (AB5675

Millipore; 1:2500 in PBS with 2% NGS, 2% bovine serum albumin (BSA), 10% milk, and 0.1% Triton X-100) overnight at room temperature. Then, sections were rinsed 3 times in PBS and incubated in biotinylated goat-anti-rabbit conjugated with horseradish peroxidase (HRP) (1:1000, Jackson Immunoresearch) in PBS with 2% NGS, 2% BSA, 10% milk, and 0.1% Triton X-100 for 1 h. After three washes of PBS, slides were exposed to the colorimetric diaminobenzidine reaction (DAB reagent, Dako) for 10 min and stopped with tap water. Sections were dehydrated and mounted with DPX mounting medium (Sigma Aldrich).

For NeuN IHC, after fixating, blocking (5% NGS and 0.5% Triton X-100 in PBS for 30 min followed by endogenous mouse IgG blocking (goat anti-mouse Fab fragment IgG, 1:50, Jackson Immunoresearch) in PBS for 1 h) and PBS washes, sections were incubated overnight with the primary antibody (mouse anti-rat NeuN, 1:2:000, Merck Millipore) with 1% NGS in PBS at room temperature. The following day, after PBS washes, sections were incubated with peroxidase-conjugated donkey anti-mouse (IgG-HRP, 1:500, Jackson Immunoresearch) with 1% NGS in PBS for 1 h. After washes of PBS, slides were exposed to the colorimetric diaminobenzidine reaction, dehydrated and mounted as described for mGluR5 staining.

Images covering the whole slices were acquired at 20X magnification with a light microscope using NIS elements software version 4.2 (Nikon Instruments). The mGluR5 immunoreactivity was semi-quantitatively assessed by calculating the integrated optical density (IOD) (*4*) in the regions of interest (i.e. striatum and cortex). The number of NeuN-positive neurons was quantified automatically after optimizing the sampling parameters

(intensity threshold, and minimum and maximum cell size) in an empirical manner under blind conditions (*21*). Image analysis was carried out using ImageJ software (National Institute of Health, USA) by an investigator blinded for treatment. All quantifications were performed bilaterally on triplicate sections of which the mean score was used for statistical analysis.

Statistical Analysis

Longitudinal analysis was performed with a linear mixed model, which did not require exclusion of animals if a measurement was missing as this method takes into account missing observations. Additionally, linear mixed models are more robust than repeated-measures ANOVAs. We fitted linear mixed models with genotype (WT and heterozygous), time (6, 9, and 13 months) and the interaction between genotype and time (genotype*time) as fixed effects. Since the interaction between subject and time (subject*time) was not significant, only subjects were included as random effect and the random intercept model applied. *Post-hoc* multiple comparison was performed with Tukey-Kramer pairwise comparisons to compare regional differences between genotypes for each time point and within genotype longitudinally.

References

1. Heikkinen T, Lehtimaki K, Vartiainen N, et al. Characterization of neurophysiological and behavioral changes, MRI brain volumetry and 1H MRS in zQ175 knock-in mouse model of Huntington's disease. *PLoS One.* 2012;7:e50717.

2. Paxinos G, Franklin K. *The mouse brain in stereotaxic coordinates*: Academic Press; 2 edition (December 8, 2003); 2003.

3. Bertoglio D, Amhaoul H, Van Eetveldt A, et al. Kainic Acid-Induced Post-Status Epilepticus Models of Temporal Lobe Epilepsy with Diverging Seizure Phenotype and Neuropathology. *Front neurol.* 2017;8.

4. Kosten L, Verhaeghe J, Verkerk R, et al. Multiprobe molecular imaging of an NMDA receptor hypofunction rat model for glutamatergic dysfunction. *Psychiatry Res Neuroimaging.* 2016;248:1-11.

SUPPLEMENTAL TABLE 1. Overview of number of WT and heterozygous Q175 animals imaged at each time point, average specific radioactivity injected, injected mass, and weight of the WT and heterozygous Q175 animals at each time point.

Age	Genotype	number of animals	Specifc radioactivity at injection (GBq/µmol)	injected mass (µg/kg)	body weight (g)
6 mo	WT	15	32.3 ± 9.8	1.31 ± 0.06	30.1 ± 1.8
	HET	16	34 ± 6.6	1.27 ± 0.05	28.7 ± 1.8
9 mo	WT	15	36.1 ± 9.6	1.16 ± 0.14	31.0 ± 2.0
	HET	12	33.6 ± 11.4	1.05 ± 0.17	27.9 ± 1.3***
13 mo	WT	12	44.7 ± 7.8	1.37 ± 0.05	32.9 ± 2.7
	HET	15	44.2 ± 7.2	1.34 ± 0.06	27.7 ± 1.5****

mo = months, WT = wild-type, HET = heterozygous. ***$p < 0.001$, ****$p < 0.0001$.

Values are expressed as mean ± SD.

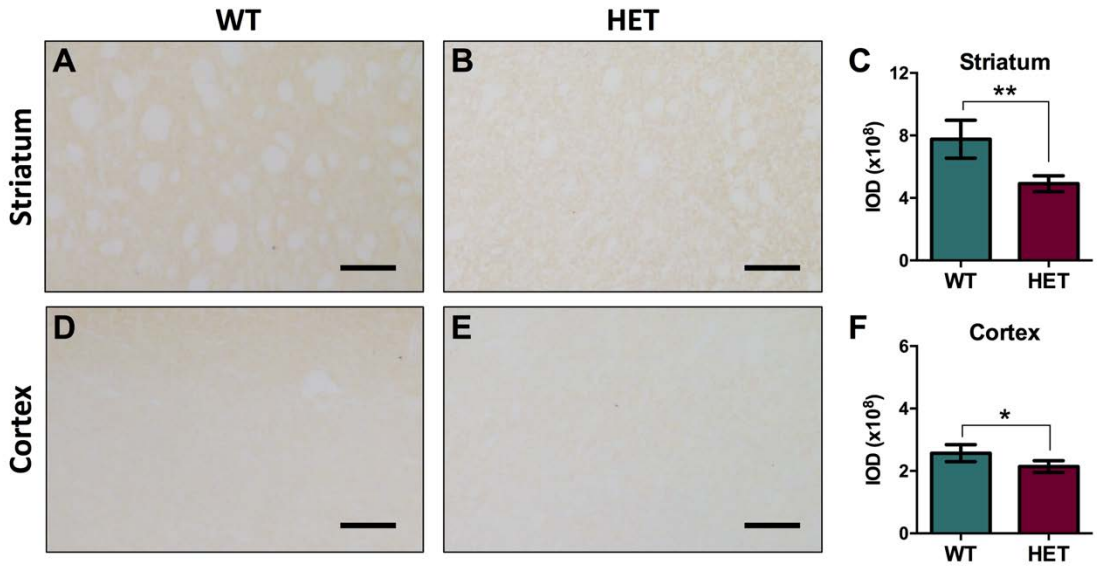

SUPPLEMENTAL FIGURE 1. mGluR5 immunoreactivity at 6 months of age. Representative images of mGluR5 immunoreactivity in striatum and cortex of WT (A and D, respectively) and heterozygous (B and E, respectively) Q175 mice. Integrated optical density showed a significant decrease in mGluR5 immunoreactivity in both striatum (C) and cortex (F) of heterozygous Q175 mice. $n = 5$ per genotype. *$p < 0.05$, **$p < 0.01$. Scale bar = 100 µm. WT = wild-type, HET = heterozygous, IOD = integrated optical density.

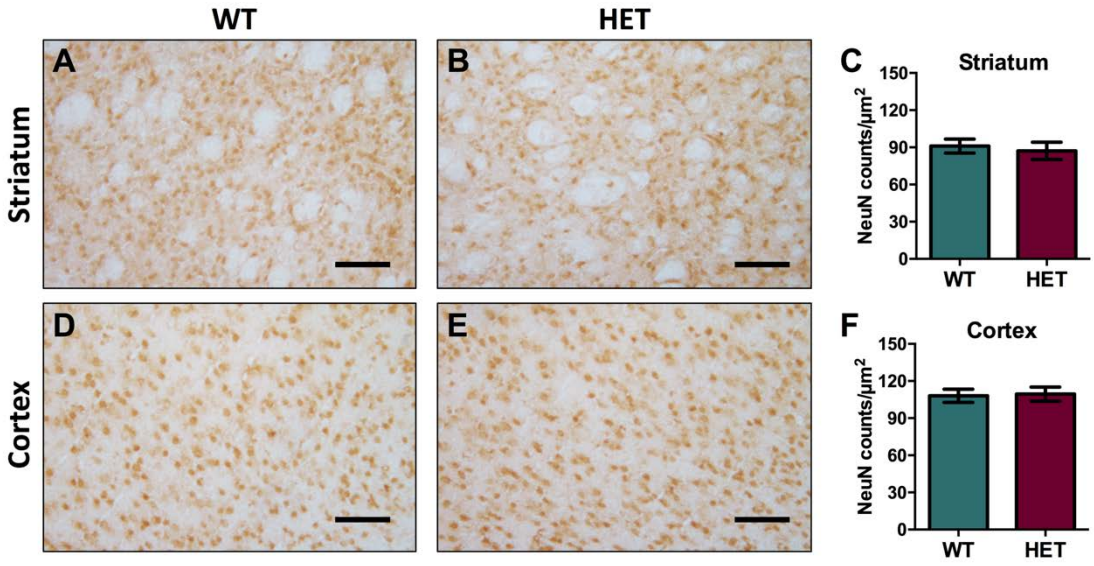

SUPPLEMENTAL FIGURE 2. Neuronal density at 6 months of age. Representative images of NeuN staining in striatum and cortex of WT (A and D, respectively) and heterozygous (B and E, respectively) Q175 mice. Neuronal count did not show any significant change between genotypes in both striatum (C) and cortex (F). *n* = 5 per genotype. Scale bar = 100 µm. WT = wild-type, HET = heterozygous.

The Journal of NUCLEAR MEDICINE

Longitudinal characterization of mGluR5 using ^{11}C-ABP688 PET imaging in the Q175 mouse model of Huntington's disease

Daniele Bertoglio, Lauren Kosten, Jeroen Verhaeghe, David Thomae, Leonie wyffels, Sigrid Stroobants, John Wityak, Celia Dominguez, Ladislav Mrzljak and Steven Staelens

J Nucl Med.
Published online: May 24, 2018.
Doi: 10.2967/jnumed.118.210658

The Journal of Nuclear Medicine is published monthly.
SNMMI | Society of Nuclear Medicine and Molecular Imaging
1850 Samuel Morse Drive, Reston, VA 20190.
(Print ISSN: 0161-5505, Online ISSN: 2159-662X)

SNMMI SOCIETY OF NUCLEAR MEDICINE AND MOLECULAR IMAGING